Hong, D., Nicolaidou, E., Hill, T. L., & Neild, S. A. (2020). Identifying phase-varying periodic behaviour in conservative nonlinear systems. *Proceedings of the Royal Society A: Mathematical, Physical and Engineering Sciences*, *476*(2237). https://doi.org/10.1098/rspa.2020.0028

PROCEEDINGS A

rspa.royalsocietypublishing.org

Research

Article submitted to journal

Subject Areas:
mechanical engineering,
mathematical modelling

Keywords:
structural dynamics, nonlinear normal modes, backbone curves, phase-amplitude coupling, reduced-order modelling

Author for correspondence:
Dongxiao Hong
e-mail: dx.hong@bristol.ac.uk

THE ROYAL SOCIETY
PUBLISHING

Identifying phase-varying periodic behaviour in conservative nonlinear systems

Dongxiao Hong, Evangelia Nicolaidou, Thomas L. Hill and Simon A. Neild

Department of Mechanical Engineering, University of Bristol, Bristol BS8 1TR, UK

Nonlinear normal modes (NNMs) are a widely used tool for studying nonlinear mechanical systems. The most commonly-observed NNMs are synchronous (i.e. single-mode, in-phase and anti-phase NNMs). Additionally, asynchronous NNMs in the form of out-of-unison motion, where the underlying linear modes have a phase difference of 90°, have also been observed. This paper extends these concepts to consider *general asynchronous NNMs*, where the modes exhibit a phase difference that is not necessarily equal to 90°. A single-mass, two-degree-of-freedom model is firstly used to demonstrate that the out-of-unison NNMs evolve to general asynchronous NNMs with the breaking of the geometrically-orthogonal structure of the system. Analytical analysis further reveals that, along with the breaking of the orthogonality, the out-of-unison NNM branches evolve into branches which exhibit amplitude-dependent phase relationships. These NNM branches are introduced here and termed *phase-varying backbone curves*. To explore this further, a model of a cable, with a support near one end, is used to demonstrate the existence of phase-varying backbone curves (and corresponding general asynchronous NNMs) in a common engineering structure.

1. Introduction

Nonlinearities in mechanical structures can cause a wide variety of complex dynamic phenomena, such as modal interactions, localisation, bifurcations and instability [1–3]. As such, identifying the existence of these phenomena, and addressing the difficulties they pose to the design, performance analysis and prediction of the behaviour of nonlinear systems can be challenging. For example,

cables can exhibit complex nonlinear behaviours [4–7]; this renders cable-supported structures, e.g. cable-stayed bridges and floating offshore systems, susceptible to unwanted vibrations during operation [8,9].

To understand these nonlinear phenomena, linear theory is often insufficient, or even invalid, since the nonlinear behaviours can significantly differ from the linearised ones. In this context, extending linear theory to account for nonlinear behaviours is needed. To address this, the concept of a Nonlinear Normal Mode (NNM) was defined by Rosenberg [10–12] as an in-unison, or a synchronous, periodic resonance for a conservative nonlinear system. It requires that the displacements of components *all* reach their extreme values and pass through equilibrium points simultaneously during periodic resonances. As such, these NNMs may be represented in terms of their initial displacements, where the initial velocities are set to zero. Such synchronous NNMs include single-mode, in-phase and anti-phase responses, which have been observed in a variety of nonlinear systems, e.g. the two-mass oscillators [13–15], beam structures [16,17], rotor systems [18], and cable structures [19].

As well as synchronous (single-mode, in-phase and anti-phase) resonances, nonlinear systems can exhibit asynchronous resonances, where the displacements of components *do not* reach their extreme values and pass through equilibrium points simultaneously while remaining periodic. To account for such asynchronous resonances, an extension to Rosenberg's definition was proposed in [20,21], where an NNM is defined as a (non-necessarily synchronous) periodic response of the conservative system; this definition of an NNM is considered throughout this paper. One example of an asynchronous NNM is the whirling motion observed in cable structures [6,19], and rotor systems [18]. This whirling motion is an out-of-unison response in which one coordinate reaches an extremum whilst another passes through the equilibrium point. As such, for a two-mode system, this motion may be represented by the initial displacement of one coordinate and the initial velocity of the other (whilst the respective initial velocity and displacement are simultaneously zero). Considering the phase of the underlying coordinates, in-phase and anti-phase motions are characterised by a phase difference of 0° or 180°, whilst out-of-unison motion is characterised by a phase difference of $\pm 90^\circ$. Besides this special case of out-of-unison motion, to the best knowledge of the authors, a more general asynchronous NNM, characterised by a general phase relationship (i.e. non-necessarily 90° out-of-phase), has not been identified in the literature. If such general asynchronous NNMs exist, they represent a large family of nonlinear responses that may affect the performance of the nonlinear systems, and may potentially be exploited. Such behaviours may be considered to be more complex than synchronous or out-of-unison motions, as they may include responses where no velocities or displacements are simultaneously zero. Their existence also indicates that the phase relationships between modal coordinates are crucial parameters to be determined when computing the NNMs.

Here, we hypothesise and then demonstrate the existence of general asynchronous NNMs using the simple motivating example of a two-mode[1] single-mass oscillator. In addition to this being a new solution type, this observation highlights the need to consider phase as a free variable (rather than constrained to 0, $\pm 90^\circ$ or 180°) when searching for NNMs using analytical techniques, and using numerical approaches that rely on systematic investigation of the initial conditions. Section 2 first revisits the concept of synchronous and asynchronous NNMs, distinguished by the phase relationships between the modal coordinates of a two-mode system with $1:1$ internal resonance. A numerical method is then used to demonstrate that the hypothisised general asynchronous NNMs can exist for the single-mass oscillator. As with the cable structure and in-line two-mass oscillator studied in [19], numerical results show that the single-mass model possesses out-of-unison NNMs when it has a geometrically-orthogonal layout. With the breaking of the orthogonal configuration, the out-of-unison NNMs can evolve to more general asynchronous cases, where the phase difference is neither 0°, 180° nor $\pm 90^\circ$. This demonstrates that such motions may exist in a nonlinear mechanical structure. Building on this finding, in Section 3, an analytical technique is used to further quantify the characteristics of

[1]Note that the term *mode* is used here to refer to a mode of the underlying linear model of the system.

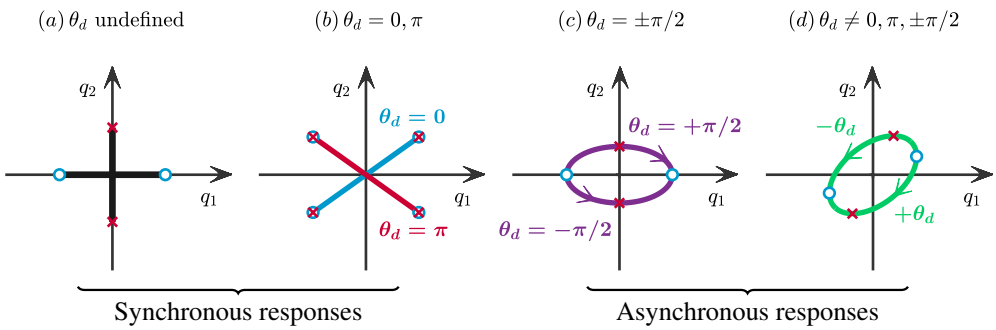

Figure 1. Schematic representations of synchronous and asynchronous nonlinear normal modes (NNMs) for a two-mode system with $1:1$ internal resonance. The responses are illustrated in the projection of the first and second linear modal coordinates, $q_1(t)$ and $q_2(t)$, parameterised in time. (a) the single-mode NNMs. (b) the in-phase ($\theta_d = 0$) and anti-phase ($\theta_d = \pi$) NNMs. (c) the $\pm\pi/2$ out-of-phase NNMs, where the '+' and '−' signs denote clockwise and anticlockwise motions respectively. (d) the $\pm\theta_d$ out-of-phase NNMs. (Online version in colour.)

asynchronous NNMs in the single-mass model. Analytical phase relationships of the backbone curves, i.e. the branches of NNMs, verify the results found in Section 2, and further reveal that, with the breaking of orthogonal configurations, the out-of-unison backbone curve evolves to one that consists of asynchronous NNMs whose phase relationships are varying along the backbone curve. This class of backbone curve is defined here as *a phase-varying backbone curve*, and represents the loci of general asynchronous NNMs.

Using insights obtained from the single-mass model, the existence of phase-varying backbone curves in a cable model (a common mechanical structure that exhibits out-of-unison backbone curves [19]) is then considered in Section 4. A reduced-order cable model is first derived and verified, using an existing analytical model [8]. The addition of a support near the cable root is then considered – this resembles the engineering practice of installing external devices to suppress vibrations [6,22,23]. This support breaks the orthogonal configuration of the cable and, as with the single-mass model, causes the out-of-unison (i.e. whirling) motions to evolve into general asynchronous motions on a phase-varying backbone curve. Finally, conclusions are presented in Section 5.

2. Nonlinear normal modes of a two-mode system with $1:1$ internal resonance

In this section, the NNMs of a two-mode system with $1:1$ internal resonance are first revisited, where an NNM is defined as a periodic response of a conservative system [20,21]. NNMs can be divided into synchronous and asynchronous solutions. Examples of the synchronous responses are shown in figure 1*a* and *b*, where the lines represent the oscillations over time in linear modal space (q_1 and q_2 denote the first and second linear modal coordinates respectively). The extrema of q_1 and q_2 are marked by 'O' and '$\times$' respectively. Figure 1*a* represents the simplest type of NNM solution – single-mode responses that contain contributions from only q_1 or q_2. Figure 1*b* shows the synchronous mixed-mode NNMs which, in contrast to the single-mode NNMs in figure 1*a*, arise from modal interactions and consist of contributions from both linear modal coordinates, q_1 and q_2. For synchronous mixed-mode NNMs, the modal coordinates reach extrema and equilibrium points simultaneously, shown in figure 1*b*. Such NNMs can be characterised using the phase relationship, θ_d, between the fundamental components of q_1 and q_2, which can be either in-phase ($\theta_d = 0$) or anti-phase ($\theta_d = \pi$); note that this phase relationship is undefined for the single-mode cases in figure 1*a*. They can also be represented by their initial modal conditions at

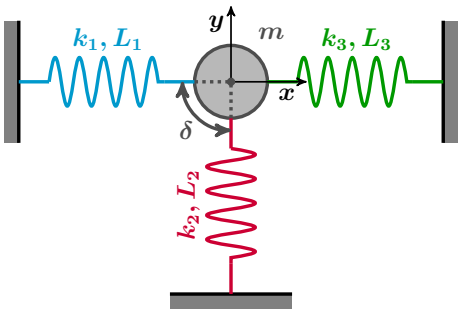

Figure 2. A schematic diagram of a single-mass, two-mode system. A mass, with mass value m, has x and y denoting horizontal and vertical in-plane displacements respectively. This mass is grounded by two horizontal springs with coefficients k_1 and k_3, and unstretched lengths L_1 and L_3. Another spring, with coefficient k_2 and unstretched length L_2, grounds the mass, with angle δ representing the angle between k_1 and k_2. The orthogonal case is shown here where $\delta = 90^\circ$ (Online version in colour.)

extrema – non-zero displacements with zero velocities. These synchronous cases can be seen in a variety of nonlinear systems – see references [13–19].

For asynchronous NNMs, an example is shown in figure 1*c* where one modal coordinate reaches an extremum when the other passes through the equilibrium point. In this case, the linear modal coordinates have $\pm\pi/2$ out-of-phase relationships (the '+' and '−' signs here denote the clockwise and anticlockwise motions respectively). Such motions can also be characterised by the initial conditions at extrema – a non-zero displacement for one coordinate with a non-zero velocity for the other, or vice versa. This class of NNM is termed an out-of-unison NNM in [19], and includes, for example, whirling motions of cables and rotor systems [18,19]. The commonly-observed NNM motions can, therefore, be categorised as single-mode (figure 1*a*, where θ_d is undefined), in-phase and anti-phase (figure 1*b*, $\theta_d = 0, \pi$ respectively) and out-of-unison (figure 1*c*, $\theta_d = \pm\pi/2$). It seems logical, therefore, to pose the question: Can other phase relationships exist between the linear modes of NNM responses? Such an NNM is depicted in figure 1*d*, and corresponds to a *general* asynchronous response where the phase relationship between linear modal coordinates is θ_d out-of-phase (to differentiate from these previously discussed cases, $\theta_d \neq 0, \pi, \pm\pi/2$). Unlike the synchronous and out-of-unison NNMs, this NNM represents responses where displacements and velocities cannot simultaneously be zero. To the knowledge of the authors, this more general asynchronous NNM has not been identified in the literature.

To explore the existence of this general asynchronous NNM, and further characterise its features, a two-mode single-mass system, schematically shown in figure 2, is firstly considered. This example system consists of one mass, with mass value m, and has displacements x and y, denoting horizontal and vertical in-plane motions respectively. This mass is grounded by three linear springs with coefficients k_1, k_2 and k_3, and with unstretched lengths L_1, L_2 and L_3 respectively. At equilibrium, all the springs are unstretched and springs, k_1 and k_3, are laying in the x-direction, whilst the angle between k_1 and k_2 is denoted δ (when $\delta = 90^\circ$, spring k_2 is orthogonal to springs k_1 and k_3). Such a system can exhibit nonlinear behaviours due to geometric nonlinearity. To investigate the nonlinear dynamic behaviours, the equations of motion can be obtained via the Euler-Lagrange equations

$$m\ddot{x} + k_1\left(L_1 + x\right) - \frac{k_1 L_1\left(L_1 + x\right)}{\sqrt{\left(L_1 + x\right)^2 + y^2}} + k_2\left[L_2\cos\left(\delta\right) + x\right] - \frac{k_2 L_2\left[L_2\cos\left(\delta\right) + x\right]}{\sqrt{\left[L_2\cos\left(\delta\right) + x\right]^2 + \left[L_2\sin\left(\delta\right) + y\right]^2}} - k_3\left(L_3 - x\right) - \frac{k_3 L_3\left(x - L_3\right)}{\sqrt{\left(L_3 - x\right)^2 + y^2}} = 0 \qquad (2.1a)$$

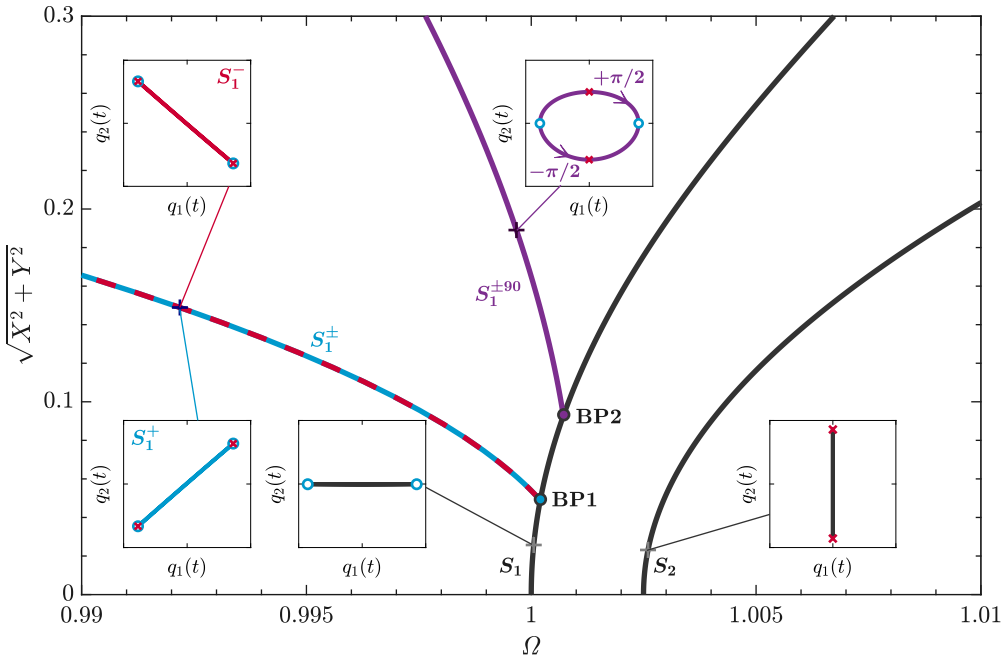

Figure 3. Backbone curves obtained via numerical continuation for the two-mode system in figure 2 with an orthogonal configuration. The backbone curves are shown as solid curves in the projection of the response frequency, Ω, against the absolute displacement of the mass, $\sqrt{X^2+Y^2}$, for a system with $m=1, k_1=k_3=0.5, k_2=1.005, L_1=L_2=L_3=1$ and $\delta=90^\circ$. Branch point bifurcations are denoted as solid dots, labelled 'BP1' and 'BP2'. Five embedded plots, in the projection of modal coordinates, $q_1(t)$ against $q_2(t)$, represent the time-parameterised responses of NNMs on the corresponding backbone curves. The extreme displacement values of modal coordinates $q_1(t)$ and $q_2(t)$ are marked by 'O' and '$\times$' respectively in these embedded plots. Arrows in the embedded plot linked to $S_1^{\pm 90}$ denote clockwise and anticlockwise motions. (Online version in colour.)

$$m\ddot{y}+k_1y-\frac{k_1L_1y}{\sqrt{(L_1+x)^2+y^2}}+k_2\left[L_2\sin(\delta)+y\right]$$
$$-\frac{k_2L_2\left[L_2\sin(\delta)+y\right]}{\sqrt{\left[L_2\cos(\delta)+x\right]^2+\left[L_2\sin(\delta)+y\right]^2}}+k_3y-\frac{k_3L_3y}{\sqrt{(L_3-x)^2+y^2}}=0. \tag{2.1b}$$

For details of the derivation, readers can refer to Appendix A. Using this two-mode model, we investigate one potential mechanism, i.e. the breaking of the orthogonality[2], that may lead to the existence of the general asynchronous resonance. This is achieved by comparing the backbone curves, i.e. branches of NNMs, for the orthogonal and non-orthogonal cases. These backbone curves are computed using the numerical continuation software COCO [24], and hence no analytical approximation is required for the results shown in this section.

(a) NNMs of the system with an orthogonal configuration

First we consider the orthogonal case, where the two-mode single-mass system has $m=1, k_1=k_3=0.5, k_2=1.005, L_1=L_2=L_3=1$ and $\delta=90^\circ$. The backbone curves of this system are shown in figure 3 in the projection of the response frequency, Ω, against the absolute displacement amplitude of the mass, $\sqrt{X^2+Y^2}$, where X and Y are the maximum amplitudes of displacements x and y respectively. In this region, there are two single-mode backbone curves

[2]Note the orthogonality here is referred to the orthogonal geometric layout of the springs.

S_1 and S_2;[3] and two mixed-mode backbone curves, S_1^+ and S_1^-, bifurcating from S_1 through the branch point bifurcation 'BP1' (the subscripts of S_1^+ and S_1^- indicate the backbone curve from which they bifurcate, in this case from S_1). Note that, due to the symmetry of the configuration, S_1^+ and S_1^- are superimposed in this projection. The NNMs on these single-mode and mixed-mode backbone curves exhibit synchronous resonances – see the time-parameterised responses of NNMs on these backbone curves in the embedded plots, which are analogous to those shown in figure 1*a* and 1*b* respectively. Besides these synchronous backbone curves, asynchronous backbone curves, i.e. the out-of-unison backbone curves, $S_1^{\pm 90}$, bifurcate from S_1 through the branch point bifurcation 'BP2'. The embedded plot, near $S_1^{\pm 90}$ in figure 3, describes the NNMs on $S_1^{\pm 90}$: q_1 reaches its extreme value when q_2 has a zero value and vice versa, and the arrows on the curve describe the clockwise motion ($\theta_d = +\pi/2$) and anticlockwise motion ($\theta_d = -\pi/2$) respectively. The out-of-unison NNMs in this plot are similar to those shown in figure 1*c*, and the out-of-unison motions reported in [19].

(b) NNMs of the system with a non-orthogonal configuration

With δ perturbed away from 90°, the orthogonality of the system is broken. The effect of breaking the orthogonality on the backbone curves is shown in figure 4 for the case where $\delta = 89.5^\circ$, whilst other parameters remain unchanged. For comparison, backbone curves for the orthogonal case are also presented using dash-dotted grey curves in this figure. It can be seen that the branch point bifurcation, 'BP1', splits to generate one primary in-phase backbone curve, S_1^+, and one isolated anti-phase backbone curve S_1^- [26]. The contribution of the first linear modal coordinate, q_1, to the single-mode backbone curve, S_2, increases from 0 and leads to an in-phase backbone curve S_2^+. These three mixed-mode backbone curves still consist of synchronous NNMs – see the embedded plots of time-parameterised responses. The other bifurcation point, 'BP2', remains, and connects the anti-phase backbone curve S_1^- to $S_1^{\pm v}$. Backbone curves, $S_1^{\pm v}$, can be seen as evolutions from the out-of-unison backbone curves, $S_1^{\pm 90}$, with the breaking of orthogonality. It is shown in the embedded plot linked to the $S_1^{\pm v}$ curves that, similar to the out-of-unison backbone curves, the NNMs on $S_1^{\pm v}$ also exhibit asynchronous responses, where the arrows denote the clockwise motion ($+\theta_d$) and anticlockwise motion ($-\theta_d$) respectively; however, the phase relationship between the two modal coordinates, θ_d, are not $\pm\pi/2$, but instead are similar to the asynchronous ones shown in figure 1*d*. This is highlighted by the dots and crosses, shown in the embedded plots, which illustrate that the extrema and equilibria are reached at different times. This demonstrates that NNMs with a general asynchronous motion can exist. The phase relationships, θ_d, of NNMs on these backbone curves show amplitude-dependent characteristics; in other words, phase relationships of NNMs are varying along the backbone curves. Hence they are termed as *phase-varying backbone curves*, denoted with the superscript '$\pm v$'. This will be discussed in detail in the next section.

In this section, the periodic responses, i.e. the NNMs, of a two-mode system with $1:1$ internal resonance were firstly reviewed, emphasising the less studied asynchronous NNMs. A specific example of such asynchronous NNMs is the out-of-unison NNM, studied in [19], where the modal coordinates have $\pm\pi/2$ phase difference. To explore the existence of a more general case, where the NNM has a phase difference $\theta_d \neq 0, \pi, \pm\pi/2$ between linear modal coordinates, a simple two-mode system, shown in figure 2, has been considered. We found that the breaking of orthogonality can transform the out-of-unison NNMs to the more general asynchronous ones. In the next section, analytical studies are carried out to further study the dynamic characteristics of the asynchronous NNMs.

[3]Note that responses on the backbone curve S_1 do contain a small component of the second mode, q_2; however, this is dominated by a response at twice the fundamental frequency and there is no component at the fundamental frequency - i.e. the motion is similar to the swaying of a cable, observed at low amplitude [25]. For consistency with later sections, we denote this as a single-mode backbone curve, representing the fact that only one mode (q_1) has a component at the fundamental frequency.

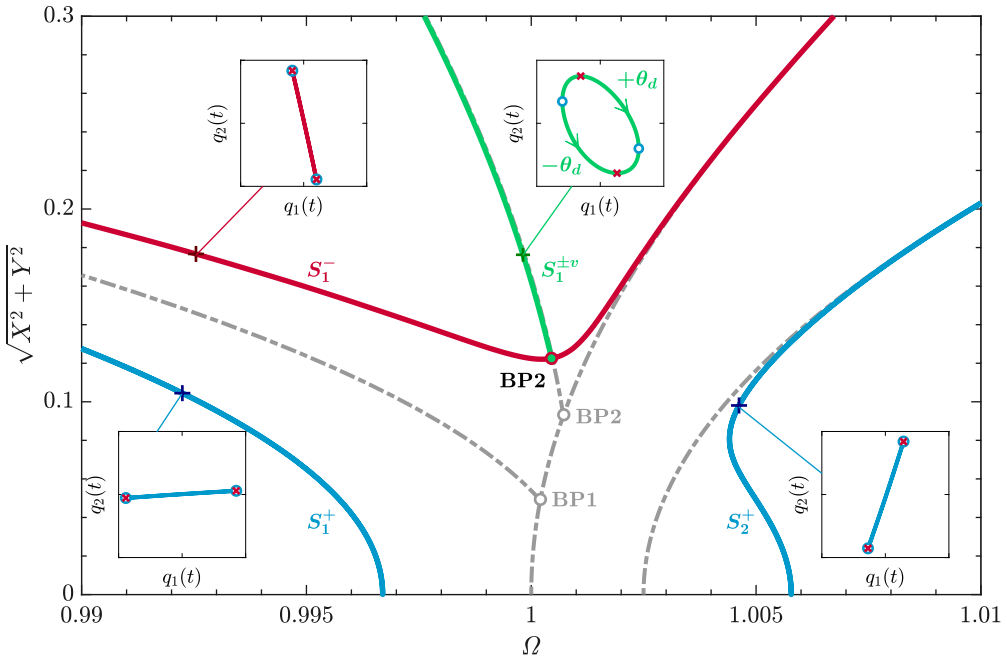

Figure 4. Backbone curves obtained via numerical continuation for the two-mode system in figure 2 with a non-orthogonal configuration. The backbone curves are shown as solid curves in the projection of the response frequency Ω against absolute displacement of the mass, $\sqrt{X^2+Y^2}$, for a system with $m=1, k_1=k_3=0.5, k_2=1.005, L_1=L_2=L_3=1$ and $\delta=89.5°$; and the branch point bifurcation is denoted as solid dot, labelled 'BP2'. Four embedded plots, in the projection of modal coordinates, $q_1(t)$ against $q_2(t)$, represent the responses of NNMs on the corresponding backbone curves. The extreme displacement values of modal coordinates $q_1(t)$ and $q_2(t)$ are marked by 'O' and '$\times$' respectively in these embedded plots. Arrows in the embedded plot linked to $S_1^{\pm v}$ denote clockwise and anticlockwise motions. For comparison, the backbone curves for the orthogonal case in figure 3 are shown as grey dash-dotted curves with branch point bifurcations denoted as hollow dots. (Online version in colour.)

3. Analytical analysis of the asynchronous backbone curves

In this section, using the harmonic balance technique, the backbone curves of the single-mass system are found analytically and further used to characterise the asynchronous responses. To simplify this analytical study, the full model, described by equations (2.1), is first expanded to a polynomial one using Maclaurin expansion, and then truncated by retaining nonlinear terms up to the cubic order. The obtained equations of motion in linear modal space are

$$\ddot{q}_1+\omega_{n1}^2q_1+3\Xi_1q_1^2+2\Xi_2q_1q_2+\Xi_3q_2^2+4\Psi_1q_1^3+3\Psi_2q_1^2q_2+2\Psi_3q_1q_2^2+\Psi_4q_2^3=0, \tag{3.1a}$$

$$\ddot{q}_2+\omega_{n2}^2q_2+\Xi_2q_1^2+2\Xi_3q_1q_2+3\Xi_4q_2^2+\Psi_2q_1^3+2\Psi_3q_1^2q_2+3\Psi_4q_1q_2^2+4\Psi_5q_2^3=0, \tag{3.1b}$$

where ω_{n1} and ω_{n2} denote the first and second linear natural frequencies respectively, and where $\Xi_1,\Xi_2,\cdots,\Xi_4$ and $\Psi_1,\Psi_2,\cdots,\Psi_5$ are quadratic and cubic nonlinear coefficients. For details of this derivation, see Appendix A.

To apply the harmonic balance method[4], it is assumed that the modal displacements may be approximated by a single harmonic, i.e.

$$q_i\approx u_i=U_i\cos\left(\omega_{ri}t-\theta_i\right), \tag{3.2}$$

[4]Other methods, such as the multiple-scales and normal form methods could alternatively be used.

where u_i represents the fundamental component of the q_i response, and where U_i, ω_{ri} and θ_i are the amplitude, frequency and phase of u_i respectively. It is further assumed that the fundamental frequencies of the two modes are equal, i.e. $\omega_{r1} = \omega_{r2} = \Omega$, which accounts for $1:1$ internal resonance. Following the procedure described in [16] – with the substitution of expressions (3.2) into the equations of motion (3.1), and the non-resonant terms removed, one can obtain the time-independent solutions from

$$4\left(\omega_{n1}^2 - \Omega^2\right)U_1 + 12\Psi_1 U_1^3 + 2\Psi_3 U_1 U_2^2\left[1+2\cos^2(\theta_d)\right] + 3\left(\Psi_4 U_2^3 + 3\Psi_2 U_1^2 U_2\right)\cos(\theta_d) = 0, \tag{3.3a}$$

$$4\left(\omega_{n2}^2 - \Omega^2\right)U_2 + 12\Psi_5 U_2^3 + 2\Psi_3 U_1^2 U_2\left[1+2\cos^2(\theta_d)\right] + 3\left(\Psi_2 U_1^3 + 3\Psi_4 U_1 U_2^2\right)\cos(\theta_d) = 0, \tag{3.3b}$$

$$\left[4\Psi_3 U_1 U_2\cos(\theta_d) + 3\Psi_2 U_1^2 + 3\Psi_4 U_2^2\right]\sin(\theta_d) = 0, \tag{3.3c}$$

where $\theta_d = \theta_1 - \theta_2$. These equations can then be used to compute the backbone curves of the two-mode system, depicted in figure 2. Note that the quadratic terms, presented in equations (3.1), do not lead to $1:1$ internally-resonant components [27], hence they do not appear in equations (3.3).

(a) Backbone curves for systems with orthogonal configurations

For orthogonal configurations of the single-mass system, one can find that $\Psi_2 = \Psi_4 = 0$ – see Appendix A for details. This further reduces equations (3.3) to

$$\left\{4\left(\omega_{n1}^2 - \Omega^2\right) + 12\Psi_1 U_1^2 + 2\Psi_3 U_2^2\left[1+2\cos^2(\theta_d)\right]\right\}U_1 = 0, \tag{3.4a}$$

$$\left\{4\left(\omega_{n2}^2 - \Omega^2\right) + 12\Psi_5 U_2^2 + 2\Psi_3 U_1^2\left[1+2\cos^2(\theta_d)\right]\right\}U_2 = 0, \tag{3.4b}$$

$$4\Psi_3 U_1 U_2\cos(\theta_d)\sin(\theta_d) = 0. \tag{3.4c}$$

There are six different sets of solutions to equations (3.4), representing the backbone curves of the system. The solution $U_1 = U_2 = 0$ is trivial, corresponding to the case where the system has no motion. Besides this trivial case, there are two single-mode solutions: one is the backbone curve, S_1, with $U_2 = 0$ and $U_1 \neq 0$; the other is the backbone curve, S_2, which has $U_1 = 0$ and $U_2 \neq 0$. Their amplitude-frequency relationships are

$$S_1: \quad U_2 = 0, \quad \Omega^2 = \omega_{n1}^2 + 3\Psi_1 U_1^2, \tag{3.5}$$

$$S_2: \quad U_1 = 0, \quad \Omega^2 = \omega_{n2}^2 + 3\Psi_5 U_2^2. \tag{3.6}$$

The NNMs on these single-mode branches, as discussed previously, are schematically shown in figure 1*a*.

Cases where $U_1 \neq 0$ and $U_2 \neq 0$ are related to mixed-mode backbone curves, hence the phase relationship (equation (3.4*c*)) between two linear modal coordinates must be determined before finding their amplitude-frequency relationships. Two sets of phase relationships can be found to satisfy equation (3.4*c*). One requires $\sin(\theta_d) = 0$, i.e. $\theta_d = n\pi$ (where $n \in \mathbb{Z}$), which corresponds to the in-phase and anti-phase cases. With $\sin(\theta_d) = 0$ substituted into equations (3.4), the amplitude-frequency relationships for in-phase and anti-phase backbone curves are given

$$S_1^{\pm},\ S_2^{\pm}\begin{cases} U_1^2 = \dfrac{2\left(\omega_{n2}^2 - \omega_{n1}^2\right) + 3\left(2\Psi_5 - \Psi_3\right)U_2^2}{3\left(2\Psi_1 - \Psi_3\right)}, \\ \Omega^2 = \dfrac{2\left(2\Psi_1\omega_{n2}^2 - \Psi_3\omega_{n1}^2\right) + 3\left(4\Psi_1\Psi_5 - \Psi_3^2\right)U_2^2}{2\left(2\Psi_1 - \Psi_3\right)}. \end{cases} \tag{3.7}$$

Like the single-mode backbone curves, NNMs on these mixed-mode, in-phase and anti-phase backbone curves relate to synchronous responses, schematically shown in figure 1*b*. Note that $S_2^{\pm}$ doesn't exist for the system considered in figure 3. The other phase relationship, satisfying

equation (3.4*c*), has $\cos(\theta_d) = 0$, i.e. $\theta_d = (2n+1)\pi/2$. This solution branch represents the out-of-unison backbone curves $S_1^{\pm 90}$ and $S_2^{\pm 90}$. Substituting $\cos(\theta_d) = 0$ into equations (3.4), the amplitude-frequency relationships of $S_1^{\pm 90}$ and $S_2^{\pm 90}$ are governed by

$$S_1^{\pm 90},\ S_2^{\pm 90} \begin{cases} U_1^2 = \dfrac{2\left(\omega_{n2}^2 - \omega_{n1}^2\right) + \left(6\Psi_5 - \Psi_3\right) U_2^2}{6\Psi_1 - \Psi_3}, \\ \Omega^2 = \dfrac{2\left(6\Psi_1\omega_{n2}^2 - \Psi_3\omega_{n1}^2\right) + \left(36\Psi_1\Psi_5 - \Psi_3^2\right) U_2^2}{2\left(6\Psi_1 - \Psi_3\right)}. \end{cases} \tag{3.8}$$

NNMs on these backbone curves exhibit $\pm\pi/2$ out-of-phase asynchronous resonances, whose responses are schematically shown in figure 1*c*. Again, we note $S_2^{\pm 90}$ doesn't exist for the system considered in figure 3.

(b) Backbone curves for systems with non-orthogonal configurations

For non-orthogonal configurations of the single-mass system, the nonlinear coefficients, Ψ_2 and Ψ_4, are not necessarily equal to 0. With non-zero values of Ψ_2 and Ψ_4, the single-mode solutions ($U_2 = 0$ and $U_1 \neq 0$, or $U_1 = 0$ and $U_2 \neq 0$) can no longer be achieved in equations (3.3). Hence, in this case, only mixed-mode backbone curves can be found. Similar to the orthogonal case, the phase relationship needs to be determined first by considering the equation (3.3*c*). This can be satisfied when $\sin(\theta_d) = 0$, i.e. $\theta_d = n\pi$, which corresponds to the in-phase and anti-phase backbone curves $S_1^{\pm}$ and $S_2^{\pm}$, similar to those discussed previously. The amplitude-frequency relationships are given by rearranging equations (3.3*a*) and (3.3*b*) as

$$S_1^{\pm},\ S_2^{\pm} \begin{cases} \Omega^2 = \omega_{n1}^2 + \dfrac{3}{4}\left[4\Psi_1 U_1^3 + 2\Psi_3 U_2^2 U_1 + p\left(\Psi_4 U_2^3 + 3\Psi_2 U_1^2 U_2\right)\right] U_1^{-1}, \\ 0 = \left(-3p\Psi_4 U_1^{-1}\right) U_2^4 + 6\left(2\Psi_5 - \Psi_3\right) U_2^3 + \left[9p\left(\Psi_4 - \Psi_2\right) U_1\right] U_2^2 + \\ \qquad \left[4\omega_{n2}^2 - 4\omega_{n1}^2 + 6\left(\Psi_3 - 2\Psi_1\right) U_1^2\right] U_2 + 3p\Psi_2 U_1^3, \end{cases} \tag{3.9}$$

where $p = \cos(n\pi)$. For even n, $p = +1$ and it indicates the in-phase backbone curves S_1^+ and S_2^+; whilst for odd n, $p = -1$, representing anti-phase backbone curves S_1^- and S_2^-.

Besides the in-phase and anti-phase cases, the other phase relationship relates to a zero value of the terms in the bracket of equation (3.3*c*), which can be rearranged as

$$\cos(\theta_d) = -\frac{3\left(\Psi_2 U_1^2 + \Psi_4 U_2^2\right)}{4\Psi_3 U_1 U_2}. \tag{3.10}$$

This expression indicates that the phase relationship (θ_d) is dependent upon the amplitude, suggesting that the phase difference between the modal coordinates is varying along the backbone curve. Here we term the asynchronous NNM branch with an amplitude-dependent phase relationship between modal coordinates as a *phase-varying backbone curve*. To find the expressions of this phase-varying backbone curve, the phase relationship (3.10) is substituted into equations (3.3*a*) and (3.3*b*), after some algebraic manipulation, one has

$$S_1^{\pm v},\ S_2^{\pm v} \begin{cases} U_1^2 = \dfrac{8\Psi_3\left(\omega_{n1}^2 - \omega_{n2}^2\right) + \left[4\Psi_3\left(\Psi_3 - 6\Psi_5\right) + 9\Psi_4\left(\Psi_4 - \Psi_2\right)\right] U_2^2}{4\Psi_3\left(\Psi_3 - 6\Psi_1\right) + 9\Psi_2\left(\Psi_2 - \Psi_4\right)}, \\ \Omega^2 = \dfrac{\left[\begin{array}{l}\left(9\Psi_2^2 - 24\Psi_3\Psi_1\right)\omega_{n2}^2 + \left(4\Psi_3^2 - 9\Psi_4\Psi_2\right)\omega_{n1}^2 \\ \quad + \left(2\Psi_3^3 - 72\Psi_1\Psi_3\Psi_5 - 9\Psi_2\Psi_3\Psi_4 + 27\Psi_1\Psi_4^2 + 27\Psi_5\Psi_2^2\right) U_2^2\end{array}\right]}{4\Psi_3\left(\Psi_3 - 6\Psi_1\right) + 9\Psi_2\left(\Psi_2 - \Psi_4\right)}. \end{cases} \tag{3.11}$$

As previously discussed, an orthogonal configuration can lead to $\Psi_2 = 0$ and $\Psi_4 = 0$. Substituting these into expressions (3.11), the amplitude-frequency relationships describing phase-varying backbone curves can be reduced to the ones describing out-of-unison backbone curves in

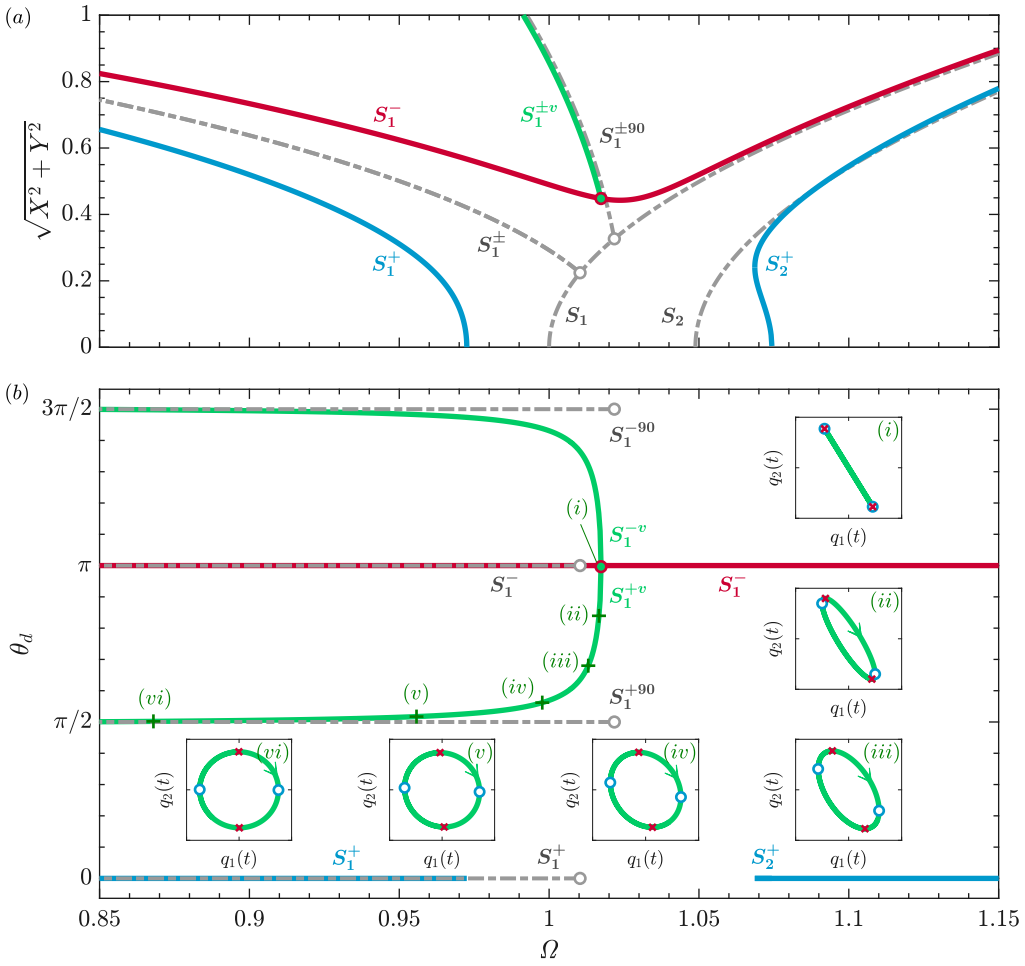

Figure 5. Analytically-computed backbone curves for the single-mass system in figure 2. The backbone curves for the orthogonal configuration, i.e. $m=1, k_1=k_3=0.5, k_2=1.1, L_1=L_2=L_3=1$ and $\delta=90^\circ$, are shown as grey dash-dotted curves; whilst the backbone curves for the system with a non-orthogonal configuration, i.e. with δ changed from 90° to 85°, are presented using solid curves. (a) Backbone curves in the projection of the response frequency, Ω, against the absolute displacement of the mass, $\sqrt{X^2+Y^2}$. (b) The phase on the backbone curves in the projection of the response frequency, Ω, against the phase difference, θ_d. Six embedded plots, in the projection of $q_1(t)$ against $q_2(t)$, show the responses, parameterised in time, of the NNMs on the phase-varying backbone curve, S_1^{+v}, positions on which are marked by the branch point bifurcation on S_1^- and '+' signs, labelled $(i), (ii), \ldots, (vi)$. The extreme values of $q_1(t)$ and $q_2(t)$, in these embedded plots, are labelled with 'O' and '×' respectively. (Online version in colour.)

equations (3.8). Furthermore, with $\Psi_2=0$ and $\Psi_4=0$, the phase relationship, described by the expression (3.10), can be reduced to $\cos(\theta_d)=0$. This phase relationship is again identical to that for the out-of-unison backbone curves. This therefore indicates that the phase-varying backbone curve is an evolution from the out-of-unison backbone curve with the orthogonality breaking, through the phase-amplitude coupling, described by equation (3.10).

Figure 5*a* presents the analytically-computed backbone curves (using equations from (3.5) to (3.11)) in the projection of the response frequency, Ω, against the absolute displacement of the mass, $\sqrt{X^2+Y^2}$, for the single-mass system in figure 2. Backbone curves for the orthogonal case (i.e. $m=1, k_1=k_3=0.5, k_2=1.1, L_1=L_2=L_3=1$ and $\theta=90^\circ$) are denoted by dash-dotted

curves; whilst backbone curves for the non-orthogonal case, obtained by changing δ from 90° to 85°, are shown as solid curves. This plot, similar to figure 4, shows the effect of breaking the orthogonality on the backbone curves. It causes the single-mode backbone curve, S_1, to split into one primary in-phase backbone curve, S_1^+, and one isolated anti-phase backbone curve S_1^-. The branch point bifurcation 'BP2' remains unsplit and the out-of-unison backbone curves, $S_1^{\pm 90}$, evolve to the phase-varying backbone curves $S_1^{\pm v}$ (two overlapping curves in this figure).

Figure 5*b* shows the phase relationships on these backbone curves in the projection of the response frequency, Ω, against the phase difference, θ_d, between the two fundamental components of modal coordinates, q_1 and q_2. For the orthogonal case, as expected, different NNMs on any one backbone curve share a fixed phase relationship between q_1 and q_2, indicated by the dash-dotted straight lines in figure 5*b*. For the non-orthogonal case, the backbone curves, S_1^+, S_1^- and S_2^+, have fixed phase relationships; however, the phase relationships of backbone curves, $S_1^{\pm v}$, vary with frequency. One branch of these phase-varying backbone curves, S_1^{+v}, has a phase relationship varying from $\theta_d = \pi$ (on the branch point bifurcation on S_1^-) to $\theta_d = \pi/2$, with the decrease in response frequency (along with the increase in displacement amplitude – see figure 5*a*). The embedded plots, labelled $(i), (ii), \ldots, (vi)$, present the time-parameterised responses of a selection of NNMs on S_1^{+v}. It can be seen that the NNMs evolve from an anti-phase NNM ($\theta_d = \pi$ on the branch point bifurcation) towards a clockwise out-of-unison NNM ($\theta_d = \pi/2$). The other phase-varying backbone, S_1^{-v}, shows similar behaviours, except for having NNMs exhibiting anticlockwise motions.

In this section, the harmonic balance technique has been used to find the analytical expressions of backbone curves for the single-mass system with orthogonal and non-orthogonal configurations. Analytical analysis shows that the general asynchronous backbone curve, discussed in Section 2, has an amplitude-dependent phase relationship between the linear modal coordinates. This backbone curve is termed as a phase-varying backbone curve, and it can be seen as an evolution from the out-of-unison backbone curve through the breaking of the orthogonality. The existence of such backbone curves indicates that phase relationships between modal coordinates are crucial parameters to be determined in finding NNMs, a key implication of which is when applying harmonic balance method numerically to compute NNMs. In the next section, numerical analysis is carried out to investigate the existence of phase-varying backbone curves in a cable model.

4. Phase-varying backbone curves for a cable model

In this section, phase-varying behaviour is investigated using a horizontal cable, taut between two fixed end points. An additional elastic support connects the cable to ground, near one of the fixed ends, as shown in figure 6. The dynamics of the cable system are modelled based on a lumped-mass approach, similar to the method in [28]. A brief description is given here for completeness.

The model is formulated by discretising the cable into n identical elastic elements, connected in series between $n+1$ nodes. The two end nodes are fixed, resulting in a total of $3(n-1)$ degrees of freedom in three-dimensional space. The mass of the cable is equally distributed between the elements, and for each element, half of its mass is lumped on either end. The elements are assumed to be undamped and linearly elastic. The cable has an unstretched length of L_0, uniform density ρ, Young's modulus E, and a constant cross-section of diameter d. Axial stress is assumed to be uniformly distributed over the cross-sectional area, and a static axial pre-tension with a horizontal component T is applied at both cable ends. The forces considered acting on the cable are due to gravity and elasticity, while viscous and aerodynamic effects are neglected.

An additional undamped, linearly elastic element is attached to the cable at a position z_s along its span. This element lies within the cross-sectional (x-y) plane, at an angle δ from the horizontal. It has a length l, stiffness k, and is unstretched when the system is at equilibrium.

A 2-DOF nonlinear reduced-order model of the cable system, which captures its salient dynamic behaviour near the first two natural frequencies, is obtained using a force-based indirect

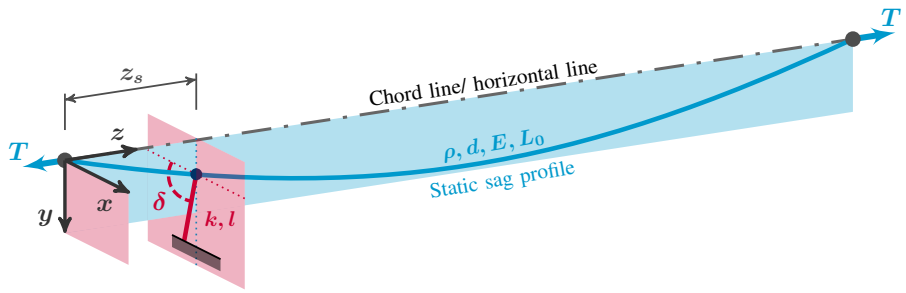

Figure 6. A schematic diagram of a cable with an unstretced length of L_0, uniform density ρ, Young's modulus E, a constant cross-section of diameter d, and a static pre-tension applied at both ends with a horizontal componen T. A physical coordinate system is defined at one end of the cable, with y-z plane denoting the cable profile, where z and y are in the direction of the chord line and the gravity respectively. An additional elastic support is attached to the cable at a position z_s along the cable span in the x-y plane, and it is modelled using a linear stiffness, k, and a support length, l, with δ indicating the angle between the support and the negative x-axis. (Online version in colour.)

reduction method [29]. This involves a projection of the equations of motion of the full model, onto a 2-DOF reduced basis. The reduction/projection basis consists of the first out-of-plane and the first in-plane transverse mass-normalised linear modeshapes of the cable about its equilibrium position. As such, the equations of motion of the reduced-order model can be written as

$$\ddot{q}_1 + \omega_{n1}^2 q_1 + f_1(q_1, q_2) = 0, \tag{4.1a}$$

$$\ddot{q}_2 + \omega_{n2}^2 q_2 + f_2(q_1, q_2) = 0, \tag{4.1b}$$

where f_1 and f_2 are the nonlinear restoring forces. For linear elastic finite element models with geometric nonlinearities, the forcing functions typically take the form of quadratic and cubic polynomials [29–31], i.e.

$$f_1(q_1, q_2) = 3\Xi_1 q_1^2 + 2\Xi_2 q_1 q_2 + \Xi_3 q_2^2 + 4\Psi_1 q_1^3 + 3\Psi_2 q_1^2 q_2 + 2\Psi_3 q_1 q_2^2 + \Psi_4 q_2^3, \tag{4.2a}$$

$$f_2(q_1, q_2) = \Xi_2 q_1^2 + 2\Xi_3 q_1 q_2 + 3\Xi_4 q_2^2 + \Psi_2 q_1^3 + 2\Psi_3 q_1^2 q_2 + 3\Psi_4 q_1 q_2^2 + 4\Psi_5 q_2^3. \tag{4.2b}$$

Note that linear dependencies are imposed on the coefficients in equations (4.2), such that the energy in the system is conserved [31,32], similar to equations (3.1).

The linear properties in equations (4.1) can be obtained directly through an eigenanalysis of the full system. However, the coefficients of the nonlinear terms in equations (4.2) are computed in a non-intrusive manner, using a set of static solutions of the lumped-mass model[5]. The static solutions are obtained by applying a set of prescribed static loads and computing the corresponding displacements. The selected loading cases consist of scaled linear combinations of the retained modes. For each load case, the computed static displacement of the full system is then projected onto the reduced modal space. Finally, the coefficients of the nonlinear terms in equations (4.2) are estimated through regression analysis in a least-squares manner, using the modal force – modal displacement dataset. A validation of the developed lumped-mass cable model, and of the corresponding reduced-order model obtained using the indirect reduction method described above, can be found in Appendix B.

We now consider a 40-element, 117-DOF cable model with the following physical parameters: $L_0 = 1.5\,\mathrm{m}$, $d = 5\,\mathrm{mm}$, $\rho = 3000\,\mathrm{kg\,m^{-3}}$, $E = 200\,\mathrm{GPa}$. The system is subjected to a static pre-tension with a horizontal component $T = 100\,\mathrm{N}$, and is additionally constrained by an elastic element with the following properties: $l = 0.2\,\mathrm{m}$, $k = 10^5\,\mathrm{N\,m^{-1}}$, and $z_s = 0.15\,\mathrm{m}$. Two additional

[5]Note that, even though the lumped-mass cable model is developed ad hoc, and the full equations of motion are known and accessible, these are not explicitly used to construct the reduced-order model as such. The indirect approach used instead, does not require knowledge of the exact equations of motion, and is applicable to finite element models built using commercial finite element software packages.

Table 1. Values of the estimated parameters of the reduced-order model for the orthogonal case, and the non-orthogonal case.

	ω_{n1}	ω_{n2}	Ξ_1	Ξ_2	Ξ_3	Ξ_4
orthogonal case	86.31	103.73	$2 \cdot 10^{-6}$	$2.72 \cdot 10^{6}$	$2 \cdot 10^{-6}$	$2.90 \cdot 10^{6}$
non-orthogonal case	87.71	102.76	$6.20 \cdot 10^{5}$	$2.58 \cdot 10^{6}$	$6.22 \cdot 10^{5}$	$2.81 \cdot 10^{6}$
	Ψ_1	Ψ_2	Ψ_3	Ψ_4	Ψ_5	
orthogonal case	$1.82 \cdot 10^{9}$	$6 \cdot 10^{-4}$	$4.09 \cdot 10^{9}$	$1 \cdot 10^{-3}$	$2.43 \cdot 10^{9}$	
non-orthogonal case	$1.86 \cdot 10^{9}$	$2.63 \cdot 10^{8}$	$4.11 \cdot 10^{9}$	$3.64 \cdot 10^{8}$	$2.38 \cdot 10^{9}$	

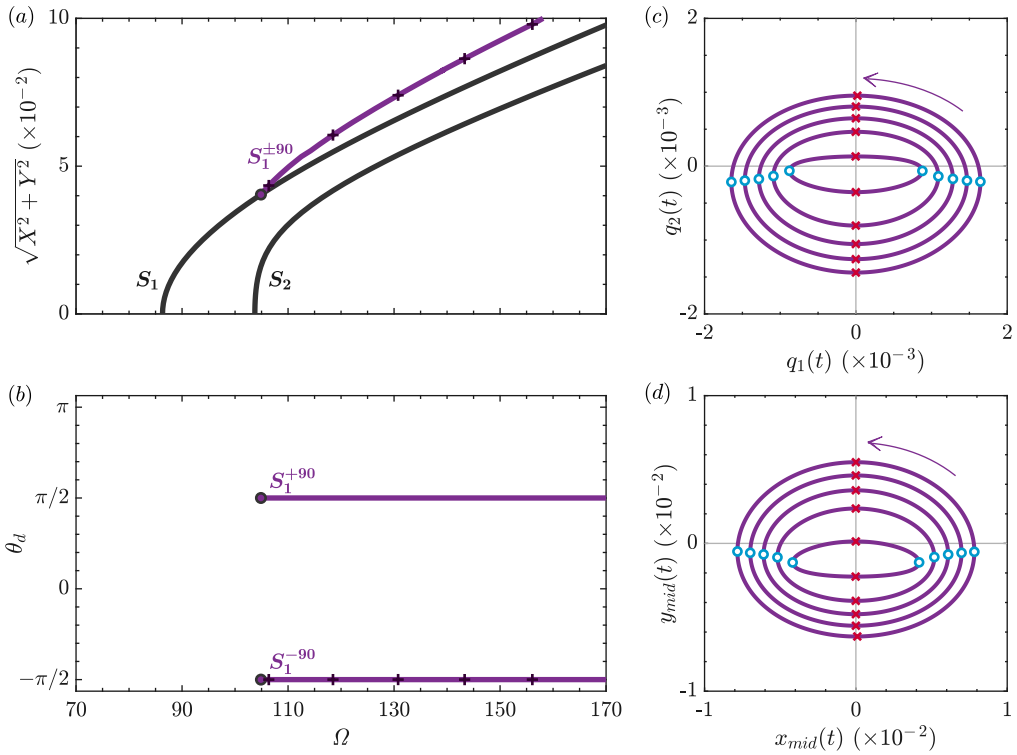

Figure 7. Numerically-computed backbone curves and responses for the cable system in figure 6 with $\delta = 90^\circ$, other modal parameters are listed in table 1. (a) Backbone curves in the projection of the response frequency, Ω, against the absolute displacement of the cable in x-y plane, $\sqrt{X^2+Y^2}$. (b) The phase on the backbone curves in the projection of the response frequency, Ω, against the phase differences between modal coordinates, θ_d. Panels (c) and (d) are the time-parameterised responses of NNMs (marked with '+' signs in panels (a) and (b)) on the out-of-unison backbone curve, S_1^{-90}, in the projection of $q_1(t)$ against $q_2(t)$, and $x_{mid}(t)$ against $y_{mid}(t)$ respectively, where x_{mid} and y_{mid} denote the physical displacements at the mid-span position in x-y plane. The extreme values of $q_1(t)$ and $x_{mid}(t)$ are labelled with 'O'; whilst the extreme values of $q_2(t)$ and $y_{mid}(t)$ are labelled with '$\times$'. The arrows in panels (c) and (d) denote the anticlockwise motions. The motions of NNMs on the other out-of-unison backbone curve, S_1^{+90}, have the same trajectories but clockwise motions. (Online version in colour.)

support layouts are considered – one corresponds to the case when the spring is aligned with the y-axis, i.e. when $\delta = 90^\circ$, and this is denoted as the orthogonal case; the other relates to the case when $\delta = 60^\circ$, and this is denoted as the non-orthogonal case. The estimated parameters of either model can be found in Table 1.

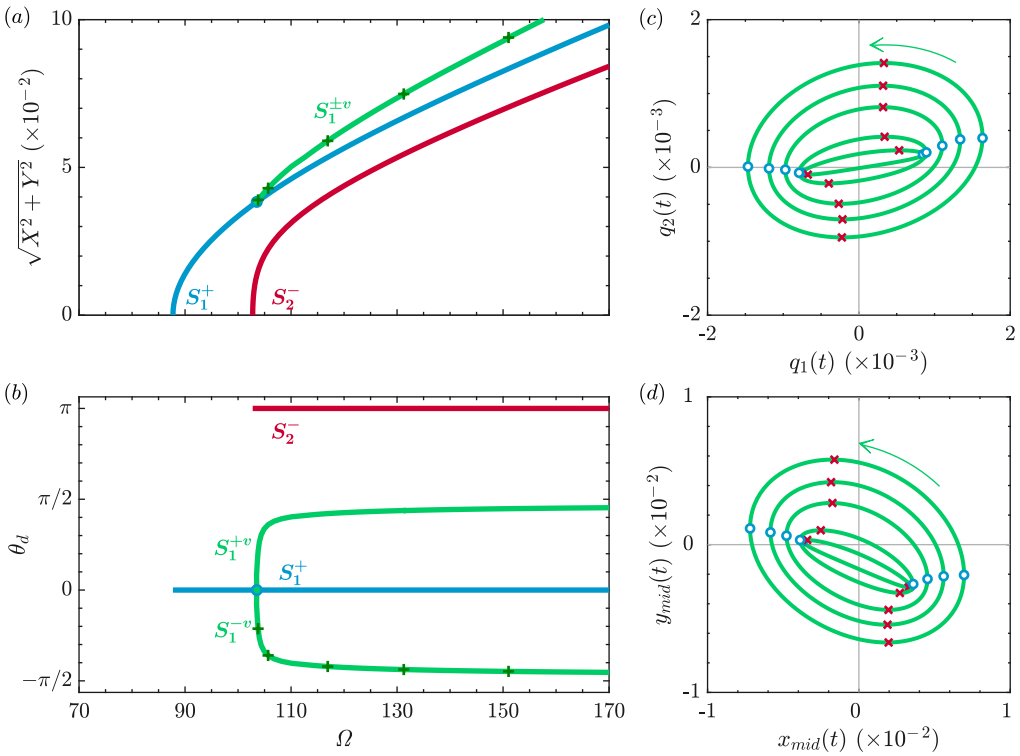

Figure 8. Numerically-computed backbone curves and responses for the cable system in figure 6 with $\delta = 60°$, other modal parameters are listed in table 1. (a) Backbone curves in the projection of the response frequency, Ω, against the absolute displacement of the cable in x-y plane, $\sqrt{X^2+Y^2}$. (b) The phase of the backbone curves in the projection of the response frequency, Ω, against the phase differences between modal coordinates, θ_d. Panels (c) and (d) are the time-parameterised responses of NNMs (marked with '+' signs in panels (a) and (b)) on the phase-varying backbone curve, S_1^{-v}, in the projection of $q_1(t)$ against $q_2(t)$, and $x_{mid}(t)$ against $y_{mid}(t)$ respectively. The extreme values of $q_1(t)$ and $x_{mid}(t)$ are labelled with 'O'; whilst the extreme values of $q_2(t)$ and $y_{mid}(t)$ are labelled with '$\times$'. The arrows in panels (c) and (d) denote the anticlockwise motions. The motions of NNMs on the other phase-varying backbone curve, S_1^{+v}, have the same trajectories but clockwise motions. (Online version in colour.)

For the orthogonal case, the backbone curves of the 2-DOF nonlinear reduced-order model of the cable system are shown in figure 7*a*. Two single-mode backbone curves can be found, namely S_1 and S_2, on which the time-parameterised responses of NNMs are similar to those shown in figure 1*a*. Besides these single-mode backbone curves, out-of-unison backbone curves, $S_1^{\pm 90}$, can also be observed. The phase relationships on these backbone curves are shown in figure 7*b*. The NNMs on either out-of-unison backbone curve exhibit a fixed phase relationship, which is represented by a straight line denoting either $\theta_d = \pm 90°$, same as the out-of-unison backbone curves for the single-mass system discussed in Section 3. A selection of NNMs on S_1^{-90}, i.e. NNMs marked by '+' signs in figures 7*a* and 7*b*, are presented in figures 7*c* and 7*d*, where the time-parameterised responses are shown in modal coordinates and physical coordinates respectively. Due to the variation of tension in cable during oscillation, a non-resonant q_2 component arises from the nonlinear quadratic terms in expressions (4.2). This leads to a shift of the extrema $q_1(t)$ (marked by 'O' in figures 7*c* and 7*d*) along the backbone curve [25]. Nonetheless, an anticlockwise out-of-unison ($\theta_d = -90°$) phase relationship between q_1 and q_2 can still be seen, similar to the one in figure 1*c*. Likewise, similar behaviours can be expected for the other out-of-unison backbone curve, S_1^{+90}, except for having clockwise motions.

Figure 8*a* shows the backbone curves for the non-orthogonal case. The corresponding phase relationships on the backbone curves are shown in figure 8*b*. With δ perturbed away from 90°, it leads the single-mode backbone curves, S_1 and S_2, to mixed-mode backbone curves, S_1^+ and S_2^-, respectively. The out-of-unison backbone curves, $S_1^{\pm 90}$, like these for the single-mass system discussed in previous sections, evolve into phase-varying backbone curves, $S_1^{\pm v}$, and bifurcate from the in-phase mixed-mode backbone curve S_1^+. The phase-varying backbone curves show phase relationships evolve from $\theta_d = 0$ (in-phase motions at the bifurcation) to $\theta_d \approx \pm\pi/2$ (nearly out-of-unison motions), as depicted in figure 8*b*. One example of this evolution of motions is presented in figure 8*c*, which describes the modal motions of NNMs marked with '+' signs on the backbone curve, S_1^{-v}, in figures 8*a* and 8*b*. Corresponding time-parameterised physical motions at the mid-span position of the cable are shown in figure 8*d*, which as well show phase-varying behaviour.

5. Conclusion

Nonlinear normal modes (NNMs) represent important tools in the analysis of nonlinear phenomena. This paper has investigated the less-commonly studied asynchronous NNMs. It has been shown that out-of-unison NNMs (characterised by a $\pm 90^\circ$ phase relationship between modal coordinates) are a special case of a more general, and previously unreported, NNM solution set where the phase relationship may assume any value. The existence of this general asynchronous NNM was first explored using a single-mass model via numerical analysis and it was demonstrated that the breaking of orthogonality causes the out-of-unison NNMs to evolve into general asynchronous NNMs (i.e. the phase difference between the modes evolves from $\pm 90^\circ$, to a general phase difference). An analytical method was then used to find the expressions of backbone curves, i.e. branches of NNMs, of the single-mass model. The analytical phase relationship between modal coordinates revealed that, along with the breaking of orthogonality, the out-of-unison backbone curves evolve to ones on which the phase relationships exhibit amplitude-dependent characteristics. This newly identified NNM branch is defined as a *phase-varying backbone curve*. The existence of phase-varying backbone curves was then investigated in a cable model, through the attachment of a near-cable-end support. This support has the effect of breaking the orthogonal geometry of the cable and, as with the single-mass example, cause the out-of-unison (whirling) motions to evolve into general asynchronous motions.

The existence of phase-varying backbone curves, and the accompanying general asynchronous NNMs, represents a new set of nonlinear phenomena in mechanical systems. These NNMs may represent significant responses in nonlinear systems, that may be critical in understanding its performance (such as the evolution from whirling in a cable with non-orthogonal geometry), or which may be exploited to improve the performance of such systems. The existence of such NNMs also indicates that phase relationships between modal coordinates are crucial parameters to be determined when computing nonlinear responses, and should be carefully considered when computing nonlinear responses. These motions may be considered more complex than the more commonly-observed synchronous or out-of-unison motions, as their displacement and velocity coordinates are never simultaneously zero. A key implication is that when using the harmonic balance technique to compute the NNMs, the phase relationships, being the critical parameters describing the nonlinear phenomena (similar to the role of the harmonic amplitudes), should be seen as unknowns to be determined.

Data Accessibility. This article has no additional data.

Authors' Contributions. D.H. led the development of the work, with supervisory support from T.L.H. and S.A.N on the development of the idea, and input from E.N. on the mathematical modelling of the cable model. All authors contributed to the preparation of the manuscript.

Competing Interests. We declare we have no competing interests.

Funding. S.A.N is supported by the EPSRC Programme grant (EP/R006768/1), D.H is supported by a scholarship from the CSC and E.N. is supported by EPSRC DTP studentship.

Acknowledgements. We gratefully acknowledge the financial support of the EPSRC and CSC.

A. Obtaining the truncated model of the single-mass system

Using ΔL_i to denote the stretch or compression of springs k_i, the Lagrangian of the one-mass two-mode system, schematically shown in figure 2, can be written as

$$\begin{aligned}\mathcal{L} =& \mathcal{T} - \mathcal{V} = \frac{1}{2}m\dot{x}^2 + \frac{1}{2}m\dot{y}^2 - \left(\frac{1}{2}k_1\left(\Delta L_1\right)^2 + \frac{1}{2}k_2\left(\Delta L_2\right)^2 + \frac{1}{2}\left(\Delta L_3\right)^2\right), \\ =& \frac{1}{2}m\dot{x}^2 + \frac{1}{2}m\dot{y}^2 - \frac{1}{2}k_1\left(\sqrt{\left(L_1+x\right)^2+y^2} - L_1\right)^2 \\ & - \frac{1}{2}k_2\left(\sqrt{\left[L_2\cos\left(\delta\right)+x\right]^2+\left[L_2\sin\left(\delta\right)+y\right]^2} - L_2\right)^2 - \frac{1}{2}k_3\left(\sqrt{\left(L_3-x\right)^2+y^2} - L_3\right)^2,\end{aligned} \tag{A.1}$$

where m is the mass value; k_1, k_2 and k_3 are the coefficients of linear springs with lengths L_1, L_2 and L_3 respectively; δ denotes the angle between springs k_1 and k_2. Applying the Euler-Lagrange equation, the equations of motion can be obtained as

$$\begin{aligned}m\ddot{x} &+ k_1\left(L_1+x\right) - \frac{k_1L_1\left(L_1+x\right)}{\sqrt{\left(L_1+x\right)^2+y^2}} + k_2\left[L_2\cos\left(\delta\right)+x\right] \\ &- \frac{k_2L_2\left[L_2\cos\left(\delta\right)+x\right]}{\sqrt{\left[L_2\cos\left(\delta\right)+x\right]^2+\left[L_2\sin\left(\delta\right)+y\right]^2}} - k_3\left(L_3-x\right) - \frac{k_3L_3\left(x-L_3\right)}{\sqrt{\left(L_3-x\right)^2+y^2}} = 0,\end{aligned} \tag{A.2a}$$

$$\begin{aligned}m\ddot{y} &+ k_1y - \frac{k_1L_1y}{\sqrt{\left(L_1+x\right)^2+y^2}} + k_2\left[L_2\sin\left(\delta\right)+y\right] \\ &- \frac{k_2L_2\left[L_2\sin\left(\delta\right)+y\right]}{\sqrt{\left[L_2\cos\left(\delta\right)+x\right]^2+\left[L_2\sin\left(\delta\right)+y\right]^2}} + k_3y - \frac{k_3L_3y}{\sqrt{\left(L_3-x\right)^2+y^2}} = 0.\end{aligned} \tag{A.2b}$$

This full model can then be expanded as polynomial equations using Maclaurin expansion, and further simplified by retaining nonlinear terms up to cubic orders. In this way, the equations of motion can be written as

$$\mathbf{M}\ddot{\mathbf{x}} + \mathbf{K}\mathbf{x} + \mathbf{N}_\mathbf{x} = \mathbf{0}, \tag{A.3}$$

where $\mathbf{M}$ and $\mathbf{K}$ are mass and linear stiffness matrices respectively; $\mathbf{N}_\mathbf{x}$ is a vector of nonlinear terms; and $\mathbf{x}$ is a vector representing physical displacements. They can be written as

$$\mathbf{M} = \begin{bmatrix} m & 0 \\ 0 & m \end{bmatrix}, \quad \mathbf{K} = \begin{bmatrix} k_1 + k_2\cos^2\left(\delta\right) + k_3 & k_2\sin\left(\delta\right)\cos\left(\delta\right) \\ k_2\sin\left(\delta\right)\cos\left(\delta\right) & k_2\sin^2\left(\delta\right) \end{bmatrix}, \tag{A.4}$$

$$\mathbf{N}_\mathbf{x} = \begin{pmatrix} 3\beta_1x^2 + 2\beta_2xy + \beta_3y^2 + 4\gamma_1x^3 + 3\gamma_2x^2y + 2\gamma_3xy^2 + \gamma_4y^3 \\ \beta_2x^2 + 2\beta_3xy + 3\beta_4y^2 + \gamma_2x^3 + 2\gamma_3x^2y + 3\gamma_4xy^2 + 4\gamma_5y^3 \end{pmatrix}, \quad \mathbf{x} = \begin{pmatrix} x \\ y \end{pmatrix}, \tag{A.5}$$

where the coefficients of nonlinear terms, $\beta_1, \beta_2, \cdots, \beta_4, \gamma_1, \gamma_2, \cdots, \gamma_5$, are

$$\begin{aligned}\beta_1 &= \frac{k_2\cos\left(\delta\right)\sin^2\left(\delta\right)}{2L_2}, \quad \beta_2 = -\frac{\left[3\cos^2\left(\delta\right)-1\right]\sin\left(\delta\right)k_2}{2L_2}, \\ \beta_3 &= -\frac{L_1L_3k_2\cos\left(\delta\right)\left[3\cos^2\left(\delta\right)-2\right] + L_3L_2k_1 - L_1L_2k_3}{2L_1L_2L_3}, \quad \beta_4 = \frac{k_2\sin\left(\delta\right)\cos^2\left(\delta\right)}{2L_2}, \\ \gamma_1 &= -\frac{\left[5\cos^2\left(\delta\right)-1\right]\sin^2\left(\delta\right)k_2}{8L_2^2}, \quad \gamma_2 = \frac{k_2\sin\left(\delta\right)\cos\left(\delta\right)\left[5\cos^2\left(\delta\right)-3\right]}{2L_2^2},\end{aligned} \tag{A.6}$$

$$\gamma_3 = -\frac{15L_1^2L_3^2k_2\cos^2(\delta)\left[\cos^2(\delta)-1\right]+2L_3^2L_2^2k_1+2L_1^2L_3^2k_2+2L_1^2L_2^2k_3}{4L_1^2L_2^2L_3^2},$$

$$\gamma_4 = -\frac{k_2\cos(\delta)\sin(\delta)\left[5\cos^2(\delta)-2\right]}{2L_2^2},$$

$$\gamma_5 = \frac{\cos^2(\delta)L_1^2L_3^2k_2\left[5\cos^2(\delta)-4\right]+L_3^2L_2^2k_1+L_1^2L_2^2k_3}{8L_1^2L_2^2L_3^2}.$$

The underlying linear model of this truncated model can be directly obtained by removing the nonlinear terms to give

$$\mathbf{M}\ddot{\mathbf{x}}+\mathbf{K}\mathbf{x}=\mathbf{0}. \tag{A.7}$$

This underlying linear model can be used for linear modal analysis to find the modal parameters, allowing the truncated system (A.3) to be translated into linear modal space. This is achieved by using substitution $\mathbf{x}=\boldsymbol{\Phi}\mathbf{q}$, where $\boldsymbol{\Phi}$ is the modeshape matrix and $\mathbf{q}$ is a vector of linear modal coordinates, written as

$$\boldsymbol{\Phi}=\begin{bmatrix}\phi_{11} & \phi_{12}\\ \phi_{21} & \phi_{22}\end{bmatrix},\quad \mathbf{q}=\begin{pmatrix}q_1\\ q_2\end{pmatrix}, \tag{A.8}$$

where the first and second columns of $\boldsymbol{\Phi}$ denote the first and second linear modeshapes respectively. After applying the linear modal transform, the equations of motion can be written

$$\ddot{\mathbf{q}}+\Lambda\mathbf{q}+\mathbf{N}_\mathbf{q}=\mathbf{0}, \tag{A.9}$$

where

$$\Lambda=\begin{bmatrix}\omega_{n1}^2 & 0\\ 0 & \omega_{n2}^2\end{bmatrix}, \tag{A.10}$$

$$\mathbf{N}_\mathbf{q}=\begin{pmatrix}3\Xi_1q_1^2+2\Xi_2q_1q_2+\Xi_3q_2^2+4\Psi_1q_1^3+3\Psi_2q_1^2q_2+2\Psi_3q_1q_2^2+\Psi_4q_2^3\\ \Xi_2q_1^2+2\Xi_3q_1q_2+3\Xi_4q_2^2+\Psi_2q_1^3+2\Psi_3q_1^2q_2+3\Psi_4q_1q_2^2+4\Psi_5q_2^3\end{pmatrix}, \tag{A.11}$$

and where ω_{ni} denotes the ith linear natural frequency, and nonlinear modal coefficients are

$$\begin{aligned}
\Xi_1 &= \beta_1\phi_{11}^3+\beta_2\phi_{11}^2\phi_{21}+\beta_3\phi_{11}\phi_{21}^2+\beta_4\phi_{21}^3,\\
\Xi_2 &= (3\beta_1\phi_{12}+\beta_2\phi_{22})\phi_{11}^2+2(\beta_2\phi_{12}+\beta_3\phi_{22})\phi_{11}\phi_{21}+(\beta_3\phi_{12}+3\beta_4\phi_{22})\phi_{21}^2,\\
\Xi_3 &= (3\beta_1\phi_{11}+\beta_2\phi_{21})\phi_{12}^2+2(\beta_2\phi_{11}+\beta_3\phi_{21})\phi_{12}\phi_{22}+(\beta_3\phi_{11}+3\beta_4\phi_{21})\phi_{22}^2,\\
\Xi_4 &= \beta_1\phi_{12}^3+\beta_2\phi_{12}^2\phi_{22}+\beta_3\phi_{12}\phi_{22}^2+\beta_4\phi_{22}^3,\\
\Psi_1 &= \gamma_1\phi_{11}^4+\gamma_2\phi_{11}^3\phi_{21}+\gamma_3\phi_{11}^2\phi_{21}^2+\gamma_4\phi_{11}\phi_{21}^3+\gamma_5\phi_{21}^4,\\
\Psi_2 &= (4\gamma_1\phi_{12}+\gamma_2\phi_{22})\phi_{11}^3+(3\gamma_2\phi_{12}+2\gamma_3\phi_{22})\phi_{11}^2\phi_{21}\\
&\quad+(2\gamma_3\phi_{12}+3\gamma_4\phi_{22})\phi_{11}\phi_{21}^2+(\gamma_4\phi_{12}+4\gamma_5\phi_{22})\phi_{21}^3,\\
\Psi_3 &= \left(6\gamma_1\phi_{12}^2+3\gamma_2\phi_{12}\phi_{22}+\gamma_3\phi_{22}^2\right)\phi_{11}^2+\left(6\gamma_5\phi_{22}^2+3\gamma_4\phi_{12}\phi_{22}+\gamma_3\phi_{12}^2\right)\phi_{21}^2\\
&\quad+\left(3\gamma_2\phi_{12}^2+4\gamma_3\phi_{12}\phi_{22}+3\gamma_4\phi_{22}^2\right)\phi_{11}\phi_{21},\\
\Psi_4 &= (4\gamma_1\phi_{11}+\gamma_2\phi_{21})\phi_{12}^3+(3\gamma_2\phi_{11}+2\gamma_3\phi_{21})\phi_{12}^2\phi_{22}\\
&\quad+(2\gamma_3\phi_{11}+3\gamma_4\phi_{21})\phi_{12}\phi_{22}^2+(\gamma_4\phi_{11}+4\gamma_5\phi_{21})\phi_{22}^3,\\
\Psi_5 &= \gamma_1\phi_{12}^4+\gamma_2\phi_{12}^3\phi_{22}+\gamma_3\phi_{12}^2\phi_{22}^2+\gamma_4\phi_{12}\phi_{22}^3+\gamma_5\phi_{22}^4.
\end{aligned} \tag{A.12}$$

Table 2. Comparison between the values of the estimated model parameters, using the analytical cable model in [8], and the 2-DOF reduced-order-model (ROM) via reduction method described in Section 4.

	ω_{n1}	ω_{n2}	Ξ_1	Ξ_2	Ξ_3	Ξ_4
cable model in [8]	122.04	123.87	0	$1.28 \cdot 10^6$	0	$1.28 \cdot 10^6$
2-DOF ROM	122.07	123.90	$1 \cdot 10^{-8}$	$1.28 \cdot 10^6$	$1 \cdot 10^{-8}$	$1.28 \cdot 10^6$
	Ψ_1	Ψ_2	Ψ_3	Ψ_4	Ψ_5	
cable model in [8]	$1.81 \cdot 10^9$	0	$3.63 \cdot 10^9$	0	$1.81 \cdot 10^9$	
2-DOF ROM	$1.81 \cdot 10^9$	$3 \cdot 10^{-7}$	$3.63 \cdot 10^9$	$1 \cdot 10^{-7}$	$1.81 \cdot 10^9$	

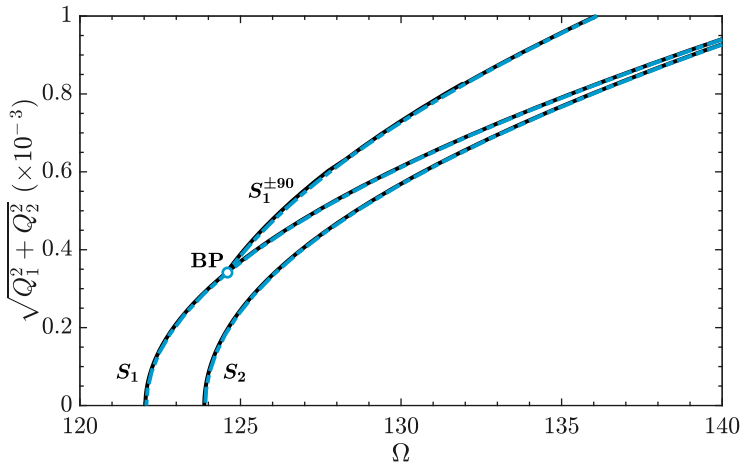

Figure 9. Comparison between the backbone curves of the 2-DOF analytically derived model in [8] (solid black line), and those of the 2-DOF reduced-order model (dash-dotted blue line) obtained using the approach described in Section 4. (Online version in colour.)

For orthogonal configurations of the single-mass system in figure 2, $\delta = 90^\circ$. Substituting $\delta = 90^\circ$ into nonlinear physical coefficients in expressions (A.6), one can find $\beta_1 = \beta_4 = \gamma_2 = \gamma_4 = 0$. Then the linear modal analysis, i.e. finding the eigenvalues and eigenvectors of $\mathbf{M^{-1}K}$, reveals that $\phi_{11} = \phi_{22}$ and $\phi_{12} = \phi_{21} = 0$. With these expressions substituted into nonlinear modal coefficients in equations (A.12), one has $\Psi_2 = \Psi_4 = 0$.

B. Validation of lumped-mass cable model and reduced-order model

The lumped-mass discretisation approach, as well as the subsequent reduction method described in Section 4, are validated by comparing the backbone curves of a reduced-order model, with those obtained using an analytically derived dynamic model of a small-sag cable system [8]. The analytical model in [8] is applicable to highly stressed cables with a small weight-to-tension ratio, such that axial modal motions can be neglected. The cable considered for validation purposes has the same properties as that described in Section 4, but the applied axial pre-tension is increased from 100 N to $T = 200$ N, in order to satisfy the aforementioned requirement.

A two-mode model based on [8] was previously studied in [19], where it was shown that the whirling motion of a cable corresponds to out-of-unison resonance between its first out-of-plane and first in-plane transverse modes. The results obtained using the corresponding reduced-order

model, are in close quantitative and qualitative agreement with these observations, as shown in Figure 9. The corresponding parameters in the equations of motion, (4.1), computed using the reduction method described in Section 4, as well as those obtained using the analytical model, are shown in Table 2.

References

1. Glendinning P. 1994 *Stability, instability and chaos: an introduction to the theory of nonlinear differential equations* vol. 11. Cambridge university press.
2. Rand RH. 2005 *Lecture notes on nonlinear vibrations*. Dept. Theoretical and Applied Mechanics, Cornell University, Ithaca, NY.
3. Pierre C, Jiang D, Shaw S. 2006 Nonlinear normal modes and their application in structural dynamics. *Mathematical Problems in Engineering* **Article ID 10847**, 15 pp.
4. Irvine HM. 1981 *Cable structures*. Cambridge, MA, U.S.A.: MIT Press.
5. Lee CL, Perkins NC. 1992 Nonlinear oscillations of suspended cables containing a two-to-one internal resonance. *Nonlinear Dynamics* **3**, 465–490.
6. Nielsen S, Krenk S. 2003 Whirling motion of a shallow cable with viscous dampers. *Journal of Sound and Vibration* **265**, 417 – 435.
7. Rega G. 2005 Nonlinear vibrations of suspended cables—Part I: Modeling and analysis. *Applied Mechanics Reviews* **57**, 443–478.
8. Warnitchai P, Fujino Y, Susumpow T. 1995 A non-linear dynamic model for cables and its application to a cable-structure system. *Journal of Sound and Vibration* **187**, 695 – 712.
9. Chen L, Basu B, Nielsen SR. 2018 A coupled finite difference mooring dynamics model for floating offshore wind turbine analysis. *Ocean Engineering* **162**, 304 – 315.
10. Rosenberg RM. 1960 Normal Modes of Nonlinear Dual-Mode Systems. *Journal of Applied Mechanics* **27**, 263–268.
11. Rosenberg RM. 1962 The Normal Modes of Nonlinear n-Degree-of-Freedom Systems. *Journal of Applied Mechanics* **29**, 7–14.
12. Rosenberg RM. 1964 On the existence of normal mode of vibrations of nonlinear systems with two degrees of freedom. *Quart. Appl. Math.* **22**, 217–234.
13. Cammarano A, Hill TL, Neild SA, Wagg DJ. 2014 Bifurcations of backbone curves for systems of coupled nonlinear two mass oscillator. *Nonlinear Dynamics* **77**, 311–320.
14. Noël JP, Detroux T, Masset L, Kerschen G, Virgin LN. 2015 Isolated Response Curves in a Base-Excited, Two-Degree-of-Freedom, Nonlinear System. In *ASME 2015 International Design Engineering Technical Conferences and Computers and Information in Engineering Conference*. American Society of Mechanical Engineers.
15. Hill TL, Cammarano A, Neild SA, Wagg DJ. 2015 Interpreting the forced responses of a two-degree-of-freedom nonlinear oscillator using backbone curves. *Journal of Sound and Vibration* **349**, 276–288.
16. Renson L, Hill TL, Ehrhardt DA, Barton DAW, Neild SA. 2018 Force appropriation of nonlinear structures. *Proceedings of the Royal Society A: Mathematical, Physical and Engineering Sciences* **474**, 20170880.
17. Ehrhardt DA, Hill TL, Neild SA. 2019 Experimentally measuring an isolated branch of Nonlinear normal modes. *Journal of Sound and Vibration* **457**, 213 – 226.
18. Yabuno H, Kashimura T, Inoue T, Ishida Y. 2011 Nonlinear normal modes and primary resonance of horizontally supported Jeffcott rotor. *Nonlinear Dynamics* **66**, 377–387.
19. Hill TL, Cammarano A, Neild SA, Wagg DJ. 2015 Out-of-unison resonance in weakly nonlinear coupled oscillators. *Proceedings of the Royal Society A: Mathematical, Physical and Engineering Sciences* **471**, 20140659.
20. Kerschen G, Peeters M, Golinval JC, Vakakis AF. 2009 Nonlinear normal modes, Part I: A useful framework for the structural dynamicist. *Mechanical Systems and Signal Processing* **23**, 170–194.
21. Peeters M, Viguié R, Sérandour G, Kerschen G, Golinval JC. 2009 Nonlinear normal modes, Part II: Toward a practical computation using numerical continuation techniques. *Mechanical Systems and Signal Processing* **23**, 195 – 216. Special Issue: Non-linear Structural Dynamics.
22. Pacheco BM, Fujino Y, Sulekh A. 1993 Estimation Curve for Modal Damping in Stay Cables with Viscous Damper. *Journal of Structural Engineering* **119**, 1961–1979.

23. Krenk S. 2000 Vibrations of a taut cable with an external damper. *Journal of Applied Mechanics* **67**, 772–776.
24. Dankowicz H, Schilder F. 2013 *Recipes for Continuation*. Philadelphia, PA: Society for Industrial and Applied Mathematics.
25. Neild SA, Champneys AR, Wagg DJ, Hill TL, Cammarano A. 2015 The use of normal forms for analysing nonlinear mechanical vibrations. *Philosophical Transactions of the Royal Society A: Mathematical, Physical and Engineering Sciences* **373**, 20140404.
26. Hong D, Hill TL, Neild SA. 2019 Conditions for the existence of isolated backbone curves. *Proceedings of the Royal Society A: Mathematical, Physical and Engineering Sciences* **475**, 20190374.
27. Touzé C. 2014 pp. 75–160. In *Normal form theory and nonlinear normal modes: Theoretical settings and applications*, pp. 75–160. Vienna: Springer Vienna.
28. Nahon M. 1999 Dynamics and control of a novel radio telescope antenna. In *Modeling and Simulation Technologies Conference and Exhibit* p. 4120.
29. Mignolet MP, Przekop A, Rizzi SA, Spottswood SM. 2013 A review of indirect/non-intrusive reduced order modeling of nonlinear geometric structures. *Journal of Sound and Vibration* **332**, 2437–2460.
30. Hollkamp JJ, Gordon RW. 2008 Reduced-order models for nonlinear response prediction: Implicit condensation and expansion. *Journal of Sound and Vibration* **318**, 1139–1153.
31. Muravyov AA, Rizzi SA. 2003 Determination of nonlinear stiffness with application to random vibration of geometrically nonlinear structures. *Computers & Structures* **81**, 1513 – 1523.
32. Tartaruga I, Elliott A, Hill TL, Neild SA, Cammarano A. 2019 The effect of nonlinear cross-coupling on reduced-order modelling. *International Journal of Non-Linear Mechanics* **116**, 7 – 17.